Electrochemistry Communications 143 (2022) 107394

Contents lists available at ScienceDirect

Electrochemistry Communications

journal homepage: www.elsevier.com/locate/elecom

Polymer of intrinsic microporosity (PIM-1) enhances hydrogen peroxide production at Gii-Sens graphene foam electrodes

Maisa Azevedo Beluomini [a,b], Yu Wang [a,c], Lina Wang [a], Mariolino Carta [d], Neil B. McKeown [e], Simon M. Wikeley [a], Tony D. James [a,f], Pablo Lozano-Sanchez [g], Marco Caffio [g], Nelson Ramos Stradiotto [b], Maria Valnice Boldrin Zanoni [b], Frank Marken [a,*]

[a] Department of Chemistry, University of Bath, Claverton Down, Bath BA2 7AY, UK
[b] Institute of Chemistry, São Paulo State University (UNESP), 14800-060 Araraquara, São Paulo, Brazil
[c] School of Material Science and Engineering, Zhengzhou University, Henan 450001, China
[d] Department of Chemistry, Swansea University, College of Science, Grove Building, Singleton Park, Swansea SA2 8PP, UK
[e] EaStChem School of Chemistry, University of Edinburgh, Edinburgh EH9 3FJ, UK
[f] School of Chemistry and Chemical Engineering, Henan Normal University, Xinxiang 453007, China
[g] Integrated Graphene Ltd., Euro House, Wellgreen Place, Stirling FK8 2DJ, UK

ARTICLE INFO

Keywords:
Graphene
Hydrogen peroxide
Generator–collector voltammetry
Disinfection
Catalysis

ABSTRACT

3D-graphene foam electrodes (Gii-Sens) immersed in a phosphate buffer solution of pH 7 are shown to generate hydrogen peroxide at a significantly faster rate in the presence of a nanoparticulate polymer of intrinsic microporosity (PIM-1). The effect is demonstrated to be associated at least in part with oxygen binding into PIM-1 under triphasic conditions. The release of the oxygen at the electrode|solution interface quadruples H_2O_2 production. Generator–collector experiments are performed with a graphene foam disk generator and a platinum disk electrode collector to allow in situ detection of hydrogen peroxide and oxygen.

1. Introduction

Polymers of intrinsic microporosity (PIMs) are molecularly rigid and contorted structures which are unable to pack and are therefore able to form films of high microporosity [1] with a typical 1000 $m^2\,g^{-1}$ surface area and typical 1 nm pore size. PIMs have found applications primarily in gas phase separation and gas binding [2], but recently have also started to attract interest in electrochemistry [3]. Interfacial redox processes that have been investigated include the CO_2 reduction [4], formic acid oxidation [5], the $Fe(CN)_6^{3-/4-}$ system [6], bound quinones [7], and the oxygen reduction reaction [8]. For the oxygen reduction reaction, the onset for formation of hydrogen peroxide was noted to be shifted to positive potentials in the presence of PIM-1 (see molecular structure in Fig. 1), indicative of a locally higher oxygen activity under triphasic conditions (gas|liquid|polymer). Electrode processes involving redox-active gases dissolved in aqueous media have been shown to be beneficially affected by the presence of polymer of intrinsic microporosity coatings on electrodes, presumably via adsorption of gas into the wet microporous structure [9]. More generally, it has recently been highlighted by Erdosy et al. [10] that a wider range of materials with intrinsic microporosity physically increase the apparent solubility of poorly water-soluble gases like oxygen under triphasic conditions.

Hydrogen peroxide production is highly sensitive to the electrode material [11]. Graphene and graphene-oxide-related materials have been shown to be active in producing hydrogen peroxide cathodically [12] but the yield of H_2O_2 may vary, dependent on conditions, defects, or doping. On exfoliated and *N*-doped graphene surfaces, oxygen reduction to H_2O_2 (the 2-electron product) is observed only as an intermediate, and reduction to H_2O (the 4-electron product) is observed in particular in acidic media [13]. The reduction mechanism on graphene surfaces is complicated by the presence of oxygen binding defects and reactive sites. On pure graphene a prominent reduction peak has been reported, linked to O_2 binding into defects in the graphene surface [14]. Here, it is demonstrated that the formation of H_2O_2 on graphene foam can be enhanced by microporous polymer deposits on the electrode surface.

A graphene foam film electrode (Gii-Sens) with approximately 40 μm foam thickness is employed [15]. This film electrode represents a

* Corresponding author.
E-mail address: f.marken@bath.ac.uk (F. Marken).

https://doi.org/10.1016/j.elecom.2022.107394
Received 21 October 2022; Received in revised form 14 November 2022; Accepted 15 November 2022
Available online 17 November 2022

substrate with a high surface area. PIM-1 is deposited either as a film (Fig. 1B) or as a nanoparticulate film (Fig. 1C). The $Fe(CN)_6^{3-/4-}$ redox probe is employed to study voltammetric behaviour in the presence of a PIM-1 film or nanoparticulate deposit. The oxygen reduction mechanism and the presence of excess oxygen (stored in PIM-1) are investigated by voltammetry and by graphene foam–platinum generator–collector electrochemistry. Preliminary evidence suggests that (a) oxygen can be accumulated/stored in PIM-1 at the electrode surface and (b) in the presence of PIM-1 the oxygen reduction mechanism is limited to the formation of the 2-electron reduction product H_2O_2.

2. Experimental

2.1. Reagents

Potassium ferricyanide (>99 %), potassium chloride (99 %), monobasic sodium phosphate (≥98.0 %), dibasic sodium phosphate (≥99.0 %), methanol and chloroform were obtained from Sigma-Aldrich and used without further purification. PIM-1 (monomer molecular weight 460 g mol^{-1}) was obtained following a method described in the literature [16]. Argon and oxygen were purchased from BOC UK (Pureshield). All solutions were prepared using deionized water (18.2 MΩ cm), obtained from a Thermo Scientific water purification system. All experiments were carried out at room temperature (20 ± 2 °C).

2.2. Instrumentation

An Autolab potentiostat system (PGSTAT12, EcoChemie, The Netherlands) was employed to control the electrochemical processes. The generator working electrode was graphene foam (4 mm diameter disk, 40 μm thick, Gii-Sens, Integrated Graphene ltd.) with a counter electrode (1 mm width ring) and a printed Ag/AgCl pseudo reference electrode. The collector electrode was a Pt disk 3 mm in diameter in a PEEK shroud. The morphological characterization of the modified electrode was performed using a scanning electron microscope (SEM, Hitachi SU3900) using an accelerating voltage of 5.0 kV. The energy-dispersive X-ray spectroscopy (EDX) unit attached to the microscope was also employed.

2.3. Procedures

PIM-1 nanoparticles were synthesized using an anti-solvent precipitation method,res as reported previously [8]. To fabricate nanoparticulate films, a volume of 5 μL (4 mg mL^{-1}) of PIM-1 solution (corresponding to 20 μg PIM-1) was dropped onto the graphene foam electrode and dried at room temperature. Dense films were obtained by deposition from chloroform solution.

2.4. Characterisation

Fig. 2 shows typical SEM images for graphene foam, graphene foam with PIM-1 nanoparticles, graphene foam with PIM-1 film, and the corresponding EDX analyses. Fig. 2A shows foam-like microstructures. In Fig. 2B the PIM-1 nanoparticles are seen spread over the graphene foam. In a previous report these particles were shown to be approximately 50 nm in diameter [8]. In Fig. 2C a PIM-1 film deposit on the graphene foam is not clearly observed in the morphology but detected based on the nitrogen content in the EDX data.

2.5. Electrode system

For generator–collector electrode experiments the graphene foam electrode was coated with a droplet of electrolyte (100 μL) and a platinum disk collector electrode was positioned face-to-face using a custom-made 3D-printed holder. Fig. 3 shows photographs of the electrode (A) and the environmental chamber (B), as well as a schematic (C). The generator–collector distance was calibrated voltammetrically using 5 mM $K_3[Fe(CN)_6]$ in aqueous 1 M KCl.

3. Results and discussion

3.1. Graphene foam–platinum generator–collector voltammetry for $Fe(CN)_6^{3-/4-}$

An aqueous solution of $Fe(CN)_6^{3-}$ is employed as a model redox system in order to characterise the graphene foam electrodes and the graphene–platinum generator–collector electrode configuration. The cyclic voltammetry data in Fig. 4A are for the one-electron reduction of 5 mM $Fe(CN)_6^{3-}$ in aqueous 1 M KCl (scan rate of 0.025 V s^{-1}) using a bare graphene foam electrode, a PIM-1 film-coated electrode, and a PIM-1 nanoparticle-coated graphene foam electrode. At the bare graphene foam electrode, an oxidation peak at 0.24 V vs Ag/AgCl and a reduction peak at 0.18 V vs Ag/AgCl suggest a midpoint potential of $E_{mid} = ½ E_{p,ox} + ½ E_{p,red} = 0.21$ V vs Ag/AgCl (Fig. 4A). In the presence of a PIM-1 film,

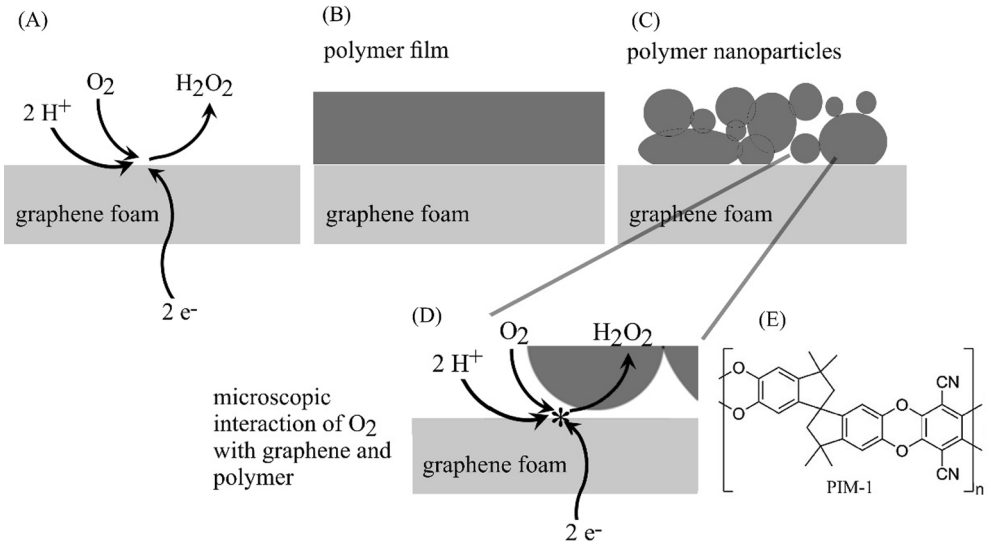

Fig. 1. Schematic illustration of (A) the 2-electron 2-proton reduction of oxygen, (B) the case of a PIM-1 film deposit, (C) the case of a nanoparticulate PIM-1 film, (D) the PIM-1|graphene interface, and (E) the molecular structure of PIM-1.

(A)

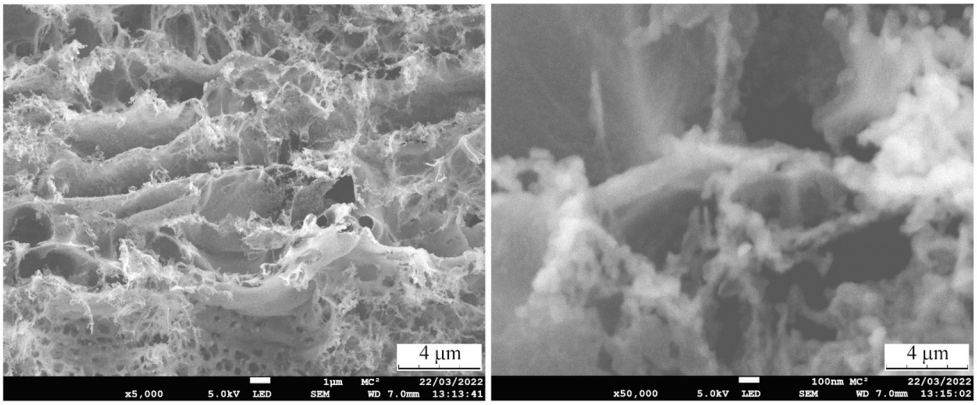

(B)

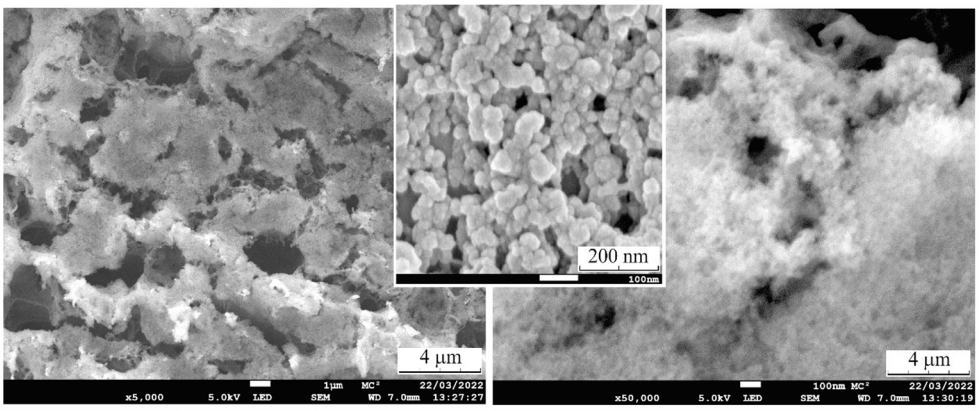

(C)

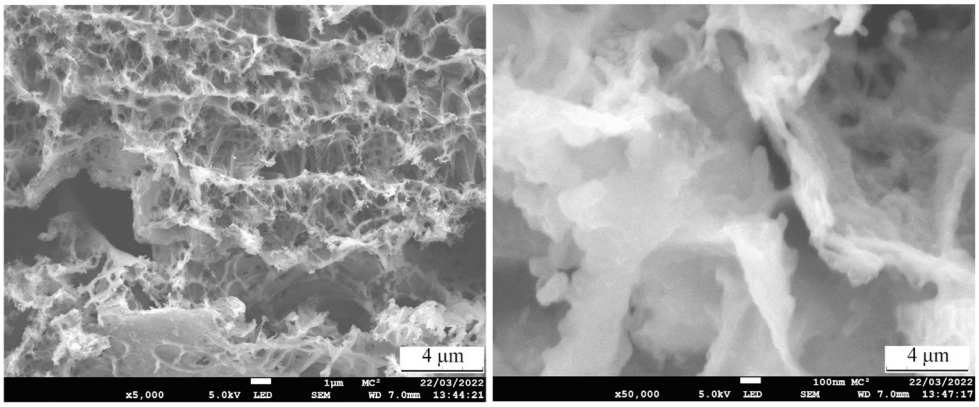

(D)

	C /%	O /%	N /%
Graphene foam	99.01	0.99	-
Graphene foam with PIM-1 nanoparticles	90.77	5.76	3.47
Graphene foam with PIM-1 film	95.66	3.37	0.97

Fig. 2. SEM images showing (A) Gii-Sens graphene foam; (B) graphene foam with PIM-1 nanoparticles (inset shows a higher magnification image of PIM-1 nanoparticles on a silicon substrate); (C) graphene foam with PIM-1 film; and (D) results of EDX analyses.

the currents are lower, presumably due to slower mass transport through the dense polymer film. However, when using a PIM-1 nanoparticle film, the current response is not significantly affected. Due to the partial blocking effect of the PIM-1 film, the focus here is on nanoparticulate PIM-1 films on the graphene foam electrode.

The peak current for the reduction of 5 mM $Fe(CN)_6^{3-}$ at the 4 mm diameter graphene foam disk is approximately 88 µA. With the known diffusion coefficient, $D_{\text{ferrocyanide}} = 0.63 \times 10^{-9}$ m^2 s^{-1} [17], $n = 1$, $F = 96487$C mol^{-1}, $A = 12.6 \times 10^{-6}$ m^2, $C = 5$ mol m^{-3}, $R = 8.31$, $T = 293$ K, scan rate $v = 0.025$ V s^{-1}, and using the Randles–Sevcik equation [18] (eqn. (1)) the peak current is predicted to be 71 µA. The measured value is approximately 88 µA, which is only slightly higher and therefore indicative of the presence of a stagnant layer within the porous graphene foam.

$$I_p = 0.446 n^{\frac{3}{2}} F^{\frac{3}{2}} AC \sqrt{\frac{Dv}{RT}} \quad (1)$$

Fig. 4B shows typical generator–collector voltammetry data. The collector electrode potential was kept fixed at 0.6 V vs Ag/AgCl. Cyclic voltammetry data for the graphene generator electrode seems essentially the same as measurements at the bare electrode. The collector currents at the platinum electrode show a sigmoidal shape and are associated with the oxidation of some of the $Fe(CN)_6^{4-}$ generated at the

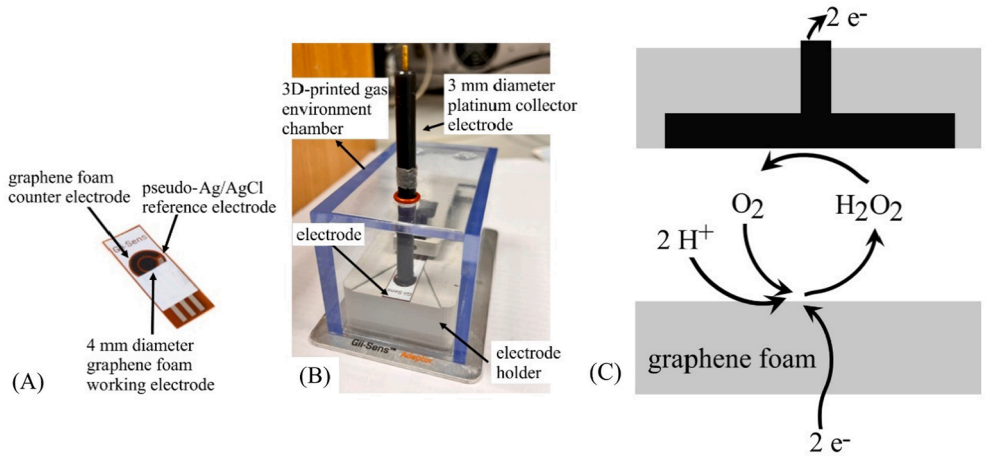

Fig. 3. Photograph of (A) the Gii-Sens graphene foam electrode and (B) holder and environmental chamber with platinum electrode inserted. (C) Schematic of the generator–collector electrode system showing O_2 reduction to H_2O_2 at the graphene foam and H_2O_2 oxidation to O_2 at the platinum electrode.

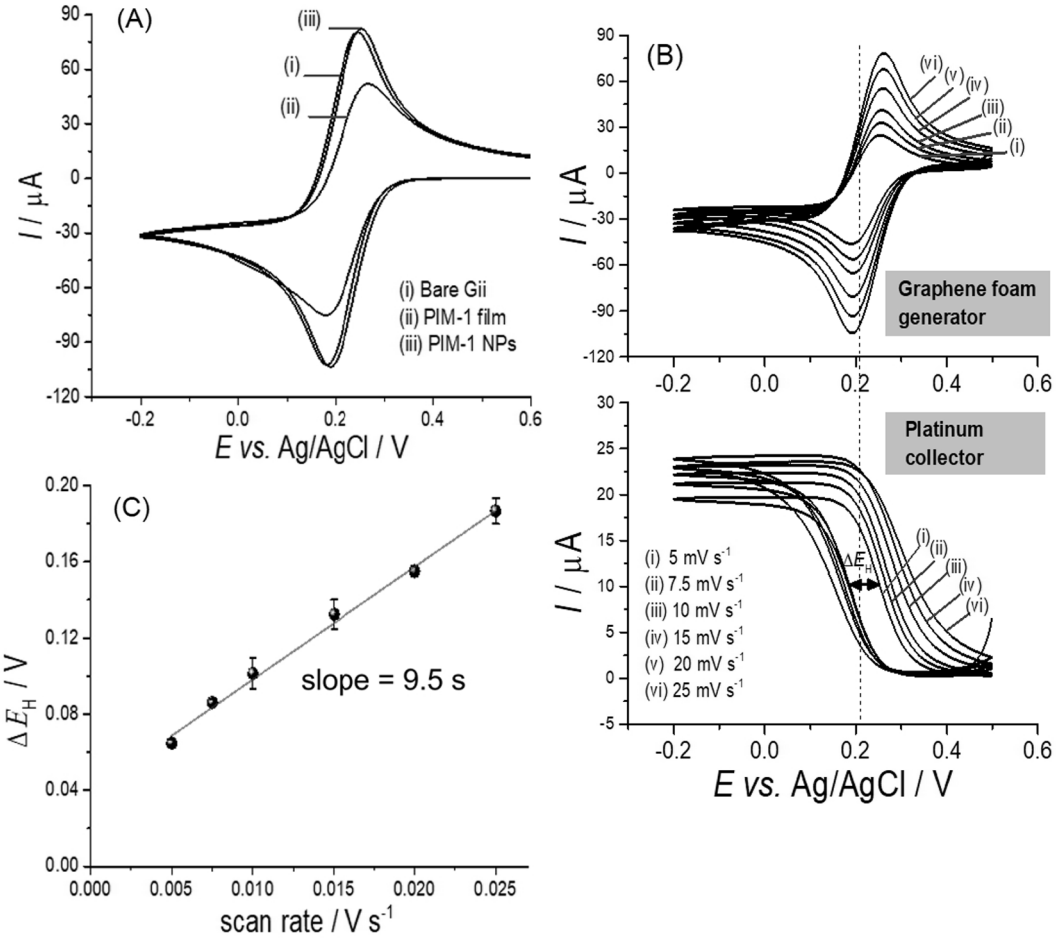

Fig. 4. (A) Cyclic voltammogram (scan rate 25 mV s^{-1}) for the reduction of 5 mM $Fe(CN)_6^{3-}$ in 1.0 M KCl on (i) bare graphene foam, (ii) dense PIM-1 film on graphene, and (iii) a PIM-1 nanoparticle film on graphene foam. (B) Graphene foam generator–platinum collector voltammetry (scan rates 5 to 25 mV s^{-1}) for 5 mM $Fe(CN)_6^{3-}$ in 1.0 M KCl solution with collector potential held at +0.6 V vs Ag/AgCl. (C) Plot of ΔE_H for the collector current versus scan rate.

graphene foam electrode. The limiting current (steady state) approaches approximately 18 µA for lower scan rates (0.005 V s^{-1}).

Both the limiting current in generator–collector mode and the potential hysteresis $\triangle E_H$ are sensitive to the distance between generator and collector electrode. A calibration can be carried out. The hysteresis effect (ΔE_H, defined here as the potential difference at half height of the current signal) at the collector electrode results from the diffusional delay [21,22] and can be represented by a linear relationship (eqn. (2)). For a one-electron redox system and assuming at least approximately $D_{ox} = D_{red}$, the gap between the two electrodes can be estimated using the following equation:

$$\Delta E_H = 0.0071 \times \nu \times \delta^2 \times \frac{F}{(DRT)} \quad (2)$$

Here $\Delta E_H = 80$ mV is the potential difference at half the collector current, ν is the scan rate, δ is the inter-electrode gap, F is the Faraday constant, D is the diffusion coefficient, R is the gas constant, and T is the absolute temperature. The calculated value for the inter-electrode distance or estimated gap size was 140 ± 20 μm. Fig. 4C shows an approximately linear dependence for ΔE_H versus scan rate with a non-zero intercept due to the porosity of the graphene foam electrode. Alternatively, the inter-electrode gap calibration can be performed by analysing the steady-state limiting current with a Nernst diffusion layer expression (eqn. (3)):

$$I_{lim} = n\,F\,A\,D\,c\,/\delta \quad (3)$$

Here the steady-state diffusional current I_{lim} is correlated with n, the number of electrons transferred per molecule diffusing to the electrode, the gap δ, the area A (collector electrode area 7.06×10^{-6} m^2), the Faraday constant F, the diffusion coefficient D, and the concentration difference c, which is equal to the bulk concentration in this case. With a limiting current of $I_{lim} = 20$ μA (see collector limiting current) this suggests an average microgap distance of approximately 100 ± 20 μm. These values for the inter-electrode distance are affected by graphene porosity and have to be regarded as estimates.

3.2. Graphene foam–platinum generator–collector voltammetry for oxygen reduction: Effects of PIM-1

The oxygen reduction reaction kinetics depend on the electrode material. The process can lead to a 2-electron product, H_2O_2, or a 4-electron product, H_2O. To compare the electrochemical reactivity of graphene foam to that of graphene foam coated with PIM-1, an aerated solution containing 0.1 mol/L phosphate buffer pH 7 was employed. Fig. 5A shows repeat cyclic voltammograms (with rinsing and drying between experiments) for graphene foam electrodes with a prominent oxygen reduction peak at −0.92 V vs Ag/AgCl. This prominent reduction peak is linked in part to the presence of defects in the graphene material [14] and is therefore associated with some oxygen binding to the graphene surface (as well as diffusion of oxygen to the surface). When repeating these cyclic voltammetry experiments without rinsing and drying, a gradual recovery of the reduction peak is noted due to slow oxygen binding to the graphene surface (Fig. 5B). In the presence of PIM-1 nanoparticles, a similar peak feature is observed with slightly enhanced and broadened current peaks (Fig. 5C).

In order to explore the oxygen reduction reaction in more detail, graphene foam–platinum generator–collector experiments are performed. At the generator electrode the potential is scanned from 0.3 to −1.3 V vs Ag/AgCl and at the platinum collector electrode a constant potential of 0.5 V vs Ag/AgCl is applied to detect the anodic response of the oxidation of hydrogen peroxide to oxygen. Fig. 6 shows the generator–collector cyclic voltammograms obtained (A) without and (B) with PIM-1 nanoparticles. At a potential of −0.75 V vs Ag/AgCl the reduction peak for oxygen is observed with a peak current of 35 μA. The Pt collector electrode shows the corresponding oxidation of H_2O_2 peaking at approximately −0.96 V vs Ag/AgCl with a peak current of 2.5 μA. Collector currents do not approach a steady state, which suggests a loss of O_2 and H_2O_2 in the inter-electrode gap, presumably due to some 4-electron reduction to H_2O. The difference in peak potential between the generating and collecting electrodes is consistent with a diffusional lag time. The second potential cycle (in red) shows that oxygen has been severely depleted. By using the peak current 2.7 μA as an approximation for the steady-state limiting current and employing eqn. (3), the apparent concentration of oxygen is obtained as 0.1 mM, which is reasonably close to the expected value of 0.18 mM given that the true steady-state current was not reached (using $\delta = 100$ μm, $n = 2$, $D_{oxygen} = 2 \times 10^{-9} m^2\ s^{-1}$ [19,20]).

When the graphene foam electrode was modified with PIM-1 nanoparticles, the generator current was slightly increased to 46 μA, consistent with some more oxygen being present. However, the collector oxidation current for H_2O_2 at the peak potential of −0.85 V vs Ag/AgCl reaches a current of 10.5 μA, which is four times higher than the value obtained in the experiment in the absence of PIM-1. These results indicate that oxygen is indeed stored in the nanoparticulate PIM-1 film and released to give rise to additional H_2O_2 production. The calculated apparent oxygen concentration (using eqn. (3)) based on the peak current is 0.4 mM, suggesting a considerable increase due to oxygen binding into PIM-1. A secondary effect of the polymer deposit at the electrode surface could be based on additional pH gradients (due to a lower buffer capacity at the polymer-coated graphene electrode surface) causing less 4-electron reduction of oxygen.

The effect of the amount of PIM-1 nanoparticle deposit on the graphene foam electrode is demonstrated in Fig. 6C. Doubling or tripling the amount of PIM-1 has only a small effect on the initial reduction peak for oxygen, but the reduction current in the potential region following the reduction peak is enhanced. The reduction peak is associated mainly

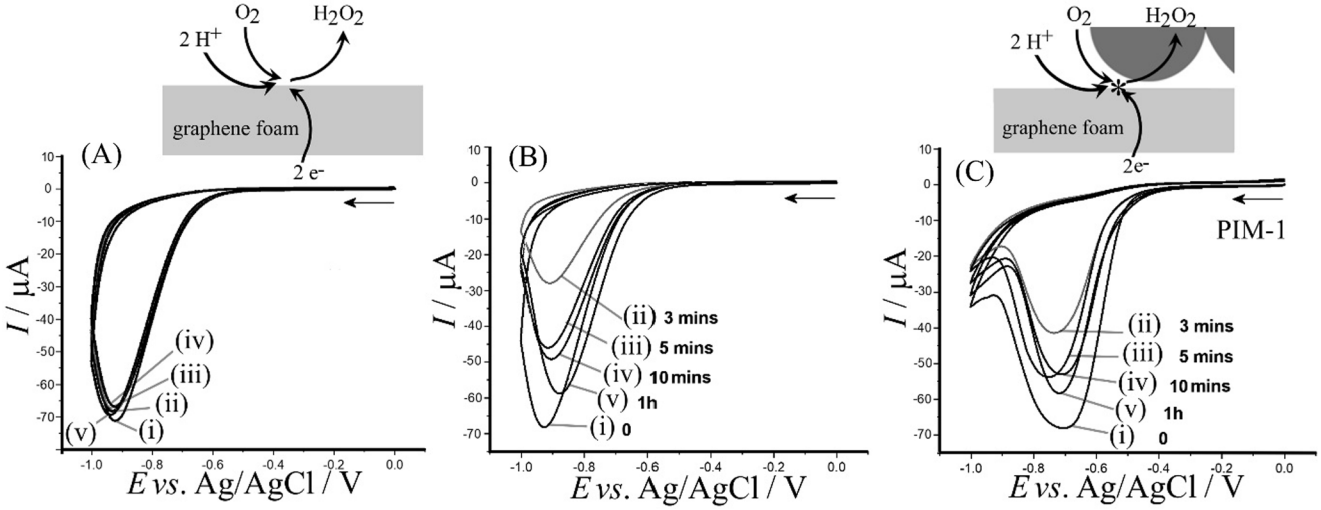

Fig. 5. (A) Cyclic voltammograms (scan rate 20 mV s^{-1}); (i) to (v) repeat experiments with rinsing and drying (between experiments) for bare graphene foam electrodes in aerated 0.1 mol/L phosphate buffer pH 7. (B–C) As before with (i) initial scan and repeat scans with a delay of (ii) 3 min, (iii) 5 min, (iv) 10 min, (v) 1 h in aerated 0.1 mol/L phosphate buffer pH 7: (B) for the bare graphene foam and (C) for PIM-1 nanoparticle-modified graphene foam.

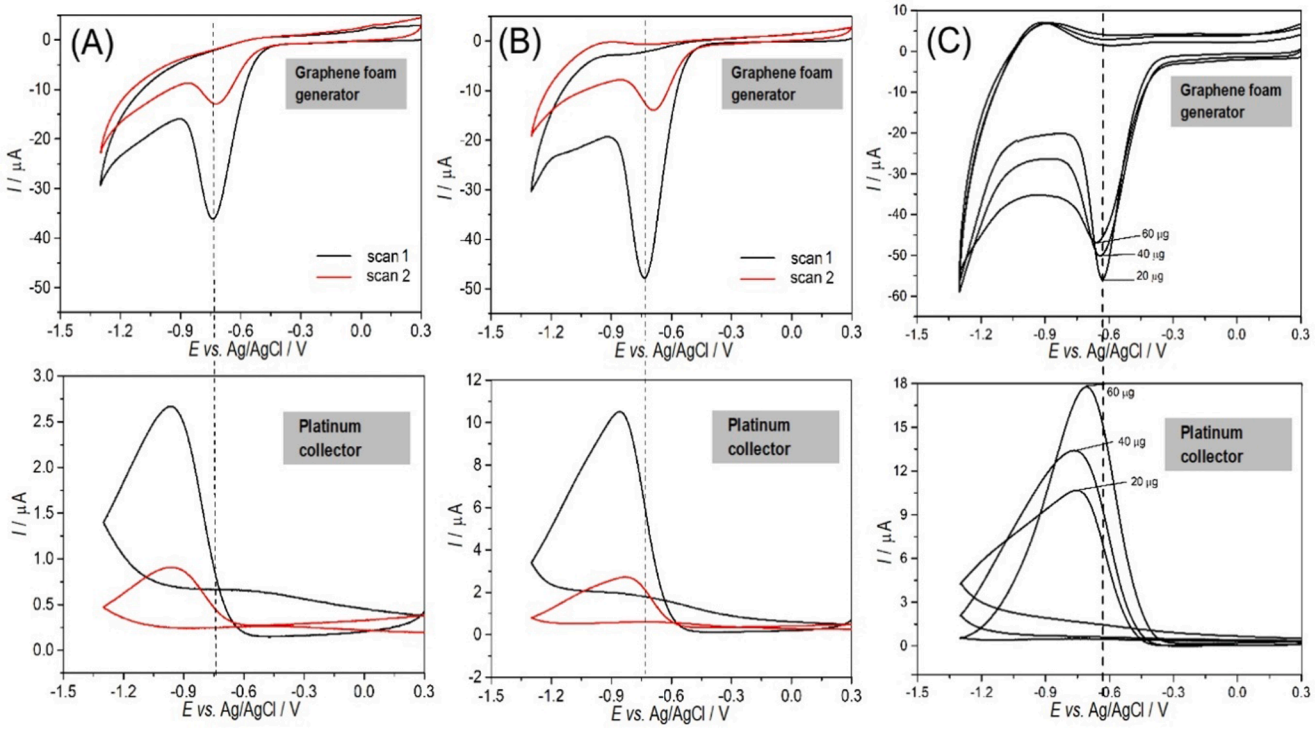

Fig. 6. (A) Graphene foam generator–platinum collector voltammograms (scan rate 10 mVs^{-1}, 0.1 mol/L phosphate buffer pH 7, collector potential fixed at 0.5 V vs Ag/AgCl.). (B) As before, but in the presence of 20 µg PIM-1 nanoparticles on the graphene foam electrode. (C) As before, but comparing deposition of 20 µg, 40 µg, and 60 µg PIM-1 nanoparticles on the graphene foam electrode.

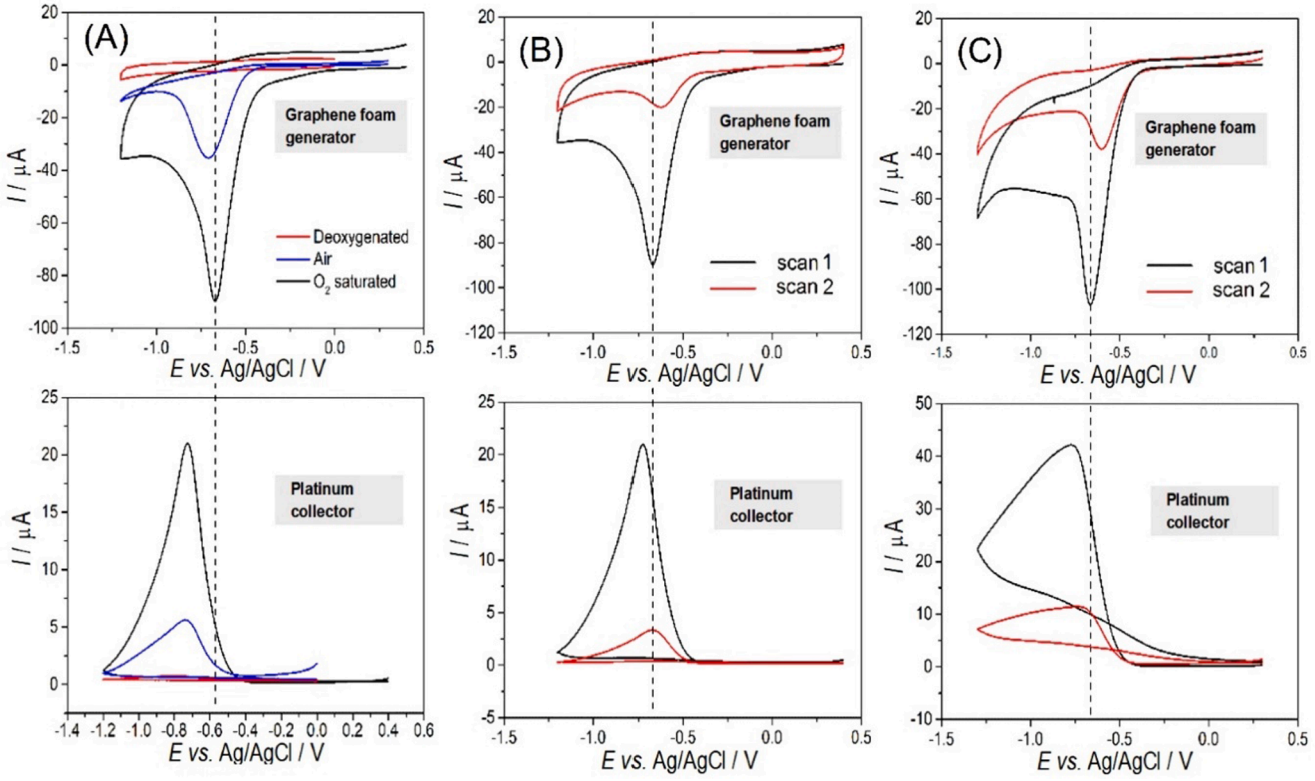

Fig. 7. Graphene foam–platinum generator–collector cyclic voltammetry (scan rate 10 mV s^{-1}, 0.1 mol/L phosphate buffer pH 7, collector potential fixed at 0.5 V vs Ag/AgCl) (A) comparing results obtained in an argon atmosphere, ambient air, and pure oxygen atmosphere. (B) As before, in a pure oxygen atmosphere without PIM-1. (C) As before, in a pure oxygen atmosphere with a PIM-1 nanoparticle deposit on graphene foam.

with oxygen adsorbed onto graphene, but the current in the potential region following the peak is associated with extraction of oxygen from the PIM-1 nanoparticles. The platinum collector electrode detects an increasing amount of H_2O_2 with more PIM-1, although the current then also decays more quickly. Using eqn. (3) and based on the peak oxidation current of 18 μA for 60 μg PIM-1, the apparent oxygen concentration is increased to 0.67 mM, which is more than three times the ambient equilibrium oxygen concentration. Under these conditions and with an ambient 80 % nitrogen atmosphere, it is likely that gas binding into the PIM-1 is dominated by nitrogen binding with only approximately 20 % oxygen binding. Therefore, experiments under a pure oxygen atmosphere are performed next.

3.3. Graphene foam–platinum generator–collector voltammetry for oxygen reduction: Oxygen concentration effects

When changing the gas environment during experiments (20 min purging with oxygen or argon gas, see Fig. 3B), effects on oxygen reduction are clearly detected. Fig. 7A shows data obtained for the graphene foam–platinum generator–collector electrode under argon, in ambient air, and in an atmosphere of pure oxygen. The reduction and oxidation processes change according to the oxygen concentration.

Fig. 7B and 7C compare the oxygen reduction in a pure oxygen atmosphere in the absence and in the presence of PIM-1 nanoparticles. In the absence of PIM-1, using the collector peak current, 22 μA, the apparent oxygen concentration is estimated as 0.8 mM, which is close to the value anticipated for pure oxygen in water. In the presence of PIM-1 the currents increase. The generator current increases from −90 μA to −107 μA and the collector peak currents change from 22 μA to 43 μA. The corresponding apparent oxygen concentration is 1.6 mM oxygen, again indicative of oxygen binding and release in the PIM-1 nanoparticle deposit. The use of the collector peak current rather than a true steady-state current is likely to lead to underestimation of the true oxygen levels.

In the inter-electrode gap of 100 μm an electrode diameter of 3 mm leads to an enclosed liquid volume of 7×10^{-10} m^3. The excess concentration of 0.6 mM oxygen (assuming 1 mM oxygen as the solubility limit in aqueous solution) suggests that approximately 0.4 nmol oxygen are bound to the PIM-1. The PIM-1 deposit of 20 μg corresponds to 43 nmol monomer units, which is significantly higher, although only a fraction of this PIM-1 will be in the inter-electrode gap. Therefore, a molecular binding interaction for the oxygen accumulated in the PIM-1 is possible but less likely. More likely seems the physical trapping of nano-scale gas bubbles (oxygen or nitrogen) within the hydrophobic micropores. Further study of the triphasic oxygen binding in the PIM-1 and the corresponding effects on electrochemical processes will be necessary.

4. Conclusions

Graphene foam electrodes can be employed for the reduction of oxygen to give the 2-electron product hydrogen peroxide, but yields are affected by (i) oxygen binding to defect states, (ii) simultaneous 4-electron reduction to water, (iii) interfacial pH gradients, and (iv) the apparent oxygen concentration. The molecularly rigid intrinsically microporous polymer PIM-1, when applied as a nanoparticulate deposit on graphene, is shown to enhance the formation of the 2-electron product (H_2O_2).

The key observation in generator–collector experiments is the presence of additional oxygen that was bound into PIM-1 at the graphene foam electrode surface. A secondary factor in the enhanced production of H_2O_2 could be additional pH gradients in the presence of the polymer coating leading to more alkaline conditions at the electrode surface and therefore less H_2O_2 transformation into H_2O. In the future, a wider range of PIM materials could be developed specifically to bind gases in high concentration under triphasic conditions to alter electrode processes (e.g. for H_2O_2 production, CO_2 reduction, N_2 reduction, or for related electroanalytical applications).

CRediT authorship contribution statement

Maisa Azevedo Beluomini: . **Yu Wang:** . **Lina Wang:** . **Mariolino Carta:** . **Neil B. McKeown:** . **Simon M. Wikeley:** . **Tony D. James:** Supervision, Writing – review & editing. **Pablo Lozano-Sanchez:** . **Marco Caffio:** . **Nelson Ramos Stradiotto:** . **Maria Valnice Boldrin Zanoni:** Supervision, Writing – review & editing. **Frank Marken:** Supervision, Conceptualization, Writing – original draft.

Declaration of Competing Interest

The authors declare that they have no known competing financial interests or personal relationships that could have appeared to influence the work reported in this paper.

Data availability

Data will be made available on request.

Acknowledgements

The authors are grateful for support from the University of Bath (UK). F.M. thanks EPSRC for support (EP/K004956/1). M.A.B. is particularly grateful for the São Paulo Research Foundation (FAPESP) for a post-doctorate scholarship (grants 2020/01822-8 and 2014/50945-4). Yu Wang thanks the China Scholarship Council for a Visiting Scholar stipend (grant number 201908410374). S.M.W. thanks EPSRC (DTP) and Integrated Graphene Ltd. for scholarship support. T.D.J. wishes to thank the Royal Society for a Wolfson Research Merit Award and the Open Research Fund of the School of Chemistry and Chemical Engineering, Henan Normal University for support (2020ZD01). We thank Dr. P.J. Fletcher (Materials & Chemical Characterisation Facility MC2, University of Bath) for help with recording electron microscopy images and data.

References

[1] L. Wang, Y. Zhao, B. Fan, M. Carta, R. Malpass-Evans, N.B. McKeown, F. Marken, Polymer of intrinsic microporosity (PIM) films and membranes in electrochemical energy storage and conversion: A mini-review, Electrochem. Commun. 118 (2020), 106798, https://doi.org/10.1016/J.ELECOM.2020.106798.

[2] N.B. McKeown, The structure-property relationships of polymers of intrinsic microporosity (PIMs), Curr. Opinion Chem. Engineer. 36 (2022), 100785, https://doi.org/10.1016/j.coche.2021.100785.

[3] E. Madrid, P. Cottis, Y. Rong, A.T. Rogers, J.M. Stone, R. Malpass-Evans, M. Carta, N.B. McKeown, F. Marken, Water desalination concept using an ionic rectifier based on a polymer of intrinsic microporosity (PIM), ChemElectroChem 3 (2015) 15849–15853, https://doi.org/10.1039/c5ta04092b.

[4] S.C. Perry, S.M. Gateman, R. Malpass-Evans, N. McKeown, M. Wegener, P. Nazarovs, J. Mauzeroll, L. Wang, C. Ponce de León, Polymers with intrinsic microporosity (PIMs) for targeted CO_2 reduction to ethylene, Chemosphere 248 (2020), 125993, https://doi.org/10.1016/j.chemosphere.2020.125993.

[5] A. Mahajan, S.K. Bhattacharya, S. Rochat, A.D. Burrows, P.J. Fletcher, Y.Y. Rong, A.B. Dalton, N.B. McKeown, F. Marken, Polymer of intrinsic microporosity (PIM-7) coating affects triphasic palladium electrocatalysis, ChemElectroChem 6 (2019) 4307–4317, https://doi.org/10.1002/celc.201801359.

[6] L. Wang, R. Malpass-Evans, M. Carta, N.B. McKeown, F. Marken, The immobilisation and reactivity of $Fe(CN)_6^{3-/4-}$ in an intrinsically microporous polyamine (PIM-EA-TB), J. Solid State Electrochem. 24 (2020) 2797–2806, https://doi.org/10.1007/S10008-020-04603-4.

[7] L. Wang, R. Malpass-Evans, M. Carta, N.B. McKeown, S.B. Reeksting, F. Marken, Catechin or quercetin guests in an intrinsically microporous polyamine (PIM-EA-TB) host: accumulation, reactivity, and release, RSC Adv. 11 (2021) 27432–27442, https://doi.org/10.1039/D1RA04543A.

[8] E. Madrid, J.P. Lowe, K.J. Msayib, N.B. McKeown, Q. Song, G.A. Attard, T. Düren, F. Marken, Triphasic nature of polymers of intrinsic microporosity induces storage and catalysis effects in hydrogen and oxygen reactivity at electrode surfaces, ChemElectroChem 6 (2019) 252–259, https://doi.org/10.1002/CELC.201800177.

[9] F. Marken, E. Madrid, Y. Zhao, M. Carta, N.B. McKeown, Polymers of intrinsic microporosity in triphasic electrochemistry: perspectives, ChemElectroChem 6 (2019) 4332–4342, https://doi.org/10.1002/CELC.201900717.

[10] D.P. Erdosy, M.B. Wenny, J. Cho, C. DelRe, M.V. Walter, F. Jimenez-Angeles, B. F. Qiao, R. Sanchez, Y.F. Peng, B.D. Polizzotti, M.O. De la Cruz, J.A. Mason, Microporous water with high gas solubilities, Nature 608 (2022) 712–717, https://doi.org/10.1038/s41586-022-05029-w.
[11] Y. Pang, H. Xie, Y. Sun, M.M. Titirici, G.L. Chai, Electrochemical oxygen reduction for H_2O_2 production: catalysts, pH effects and mechanisms, J. Mater. Chem. A 8 (2020) 24996–25016, https://doi.org/10.1039/D0TA09122G.
[12] T. Yu, C.B. Breslin, Review—2D graphene and graphene-like materials and their promising applications in the generation of hydrogen peroxide, J. Electrochem. Soc. 167 (12) (2020) 126502.
[13] K.R. Lee, K.U. Lee, J.W. Lee, B.T. Ahn, S.I. Woo, Electrochemical oxygen reduction on nitrogen doped graphene sheets in acid media, Electrochem. Commun. 12 (2010) 1052–1055, https://doi.org/10.1016/J.ELECOM.2010.05.023.
[14] Y.Q. Wang, F. Grote, Q. Cao, S. Eigler, Regiochemically oxo-functionalized graphene, guided by defect sites, as catalyst for oxygen reduction to hydrogen peroxide, J. Phys. Chem. Lett. 12 (2021) 10009–10014, https://doi.org/10.1021/acs.jpclett.1c02957.
[15] S.M. Wikeley, J. Przybylowski, P. Lozano-Sanchez, M. Caffio, T.D. James, S.D. Bull, P.J. Fletcher, F. Marken, Polymer indicator displacement assay: electrochemical glucose monitoring based on boronic acid receptors and graphene foam competitively binding with poly-nordihydroguaiaretic acid, Analyst 147 (2022) 661–670, https://doi.org/10.1039/d1an01991k.
[16] P.M. Budd, E.S. Elabas, B.S. Ghanem, S. Makhseed, N.B. McKeown, K.J. Msayib, C. E. Tattershall, D. Wang, Solution-processed, organophilic membrane derived from a polymer of intrinsic microporosity, Adv. Mater. 16 (2004) 456–459, https://doi.org/10.1002/adma.200306053.
[17] R.N. Adams, Electrochemistry at Solid Electrodes, Marcel Dekker, New York, 1969, p. 220.
[18] R. Compton, C.E. Banks, Understanding Voltammetry, World Scientific London, 2007, p. 121.
[19] J. Weber, A.J. Wain, F. Marken, Microwire chronoamperometric determination of concentration, diffusivity, and salinity for simultaneous oxygen and proton reduction, Electroanalysis 27 (2015) 1829–1835, https://doi.org/10.1002/elan.201500190.
[20] M.K. Tham, R.D. Walker, K.E. Gubbins, Diffusion of oxygen and hydrogen in aqueous potassium hydroxide solutions, J. Phys. Chem. 74 (1970) 1747–1750, https://doi.org/10.1021/j100703a015.